Monthly Notices
of the
ROYAL ASTRONOMICAL SOCIETY

MNRAS **479,** 5678–5685 (2018)
Advance Access publication 2018 July 4

doi:10.1093/mnras/sty1768

On the shape and evolution of a cosmic-ray-regulated galaxy-wide stellar initial mass function

Fabio Fontanot,[1]★ Francesco La Barbera,[2] Gabriella De Lucia,[1] Anna Pasquali[3] and Alexandre Vazdekis[4,5]

[1]*INAF – Astronomical Observatory of Trieste, via G.B. Tiepolo 11, I-34143 Trieste, Italy*
[2]*INAF – Astronomical Observatory of Capodimonte, sal. Moiariello, 16, I-80131 Napoli, Italy*
[3]*Astronomisches Rechen-Institut, Zentrum für Astronomie, Universität Heidelberg, Mönchhofstr. 12-14, D-69120 Heidelberg, Germany*
[4]*Instituto de Astrofísica de Canarias, E-38200 La Laguna, Tenerife, Spain*
[5]*Departamento de Astrofísica, Universidad de La Laguna, E-38205 La Laguna, Tenerife, Spain*

Accepted 2018 July 1. Received 2018 June 29; in original form 2018 May 31

ABSTRACT

In this paper, we present a new derivation of the shape and evolution of the integrated galaxy-wide initial mass function (IGIMF), incorporating explicitly the effects of cosmic rays (CRs) as regulators of the chemical and thermal state of the gas in the dense cores of molecular clouds. We predict the shape of the IGIMF as a function of star formation rate and CR density and show that it can be significantly different with respect to local estimates. In particular, we focus on the physical conditions corresponding to IGIMF shapes that are *simultaneously* shallower at high-mass end *and* steeper at the low-mass end than those of a Kroupa IMF. These solutions can explain both the levels of α-enrichment and the excess of low-mass stars as a function of stellar mass, observed for local spheroidal galaxies. As a preliminary test of our scenario, we use idealized star formation histories to estimate the mean IMF shape for galaxies of different $z = 0$ stellar mass. We show that the fraction of low-mass stars as a function of galaxy stellar mass predicted by these mean IMFs agrees with the values derived from high-resolution spectroscopic surveys.

Key words: galaxies: evolution – galaxies: fundamental parameters – galaxies: stellar content.

1 INTRODUCTION

In recent years, a wealth of observations has challenged the notion of a universal stellar initial mass function (IMF) in early-type galaxies (ETGs), pointing to possible variations as a function of galaxy properties such as stellar mass ($M_\star$) or velocity dispersion (σ). Dynamical studies (see e.g. Treu et al. 2010; Cappellari et al. 2012; Dutton et al. 2013) suggest a systematic excess of the mass-to-light ratios derived using integral field stellar kinematics with respect to the values estimated from photometry assuming a Milky-Way (MW)-like (e.g. Kroupa or Chabrier) IMF. The excess is found to increase with σ. It is important to stress that the dynamical analysis is not able to disentangle (see e.g. Tortora, La Barbera & Napolitano 2016) between a 'top-heavy' and a 'bottom-heavy' scenario, where the excess of stellar mass is due to an enhanced fraction of either stellar remnants (from exploding supernovae, SNe) or low-mass stars.

Spectroscopy can provide an alternative and more specific approach to study IMF variations, by taking advantage of spectral features, such as, e.g. the Na I doublet at $\lambda\lambda$8183, 8195 Å (hereafter NaI8200; Faber & French 1980; Schiavon, Barbuy & Singh 1997), the TiO1 and TiO2 (Trager et al. 1998) features ($\lambda\lambda$6000, 6300 Å), and the Wing–Ford FeH band (Wing & Ford 1969; Schiavon et al. 1997) at 9900 Å. These features depend on the IMF, because of their sensitivity to stellar surface gravity and/or effective temperature,[1] and bear information on the ratio between the total number of dwarf ($m_\star \lesssim 0.5\,M_\odot$) and more massive stars ($m_\star \gtrsim 0.5\,M_\odot$). In order to extract this information from high signal-to-noise ratio spectra, a comparison with predictions from stellar population synthesis models is required. Using this technique, several studies have reported an excess of low- relative to high-mass stars in the IMF of massive ETGs, i.e. a bottom-heavy IMF. The slope at the low-mass end becomes increasingly steeper (in some cases 'super'-Salpeter, i.e. with a dwarf-to-giant ratio exceeding that of a Salpeter IMF) at

★ E-mail: fabio.fontanot@inaf.it

[1]Some features, like NaI8200, are specifically sensitive to surface gravity and thus to the IMF shape, while other indices, like TiO2, increase with decreasing stellar effective temperature. Therefore, their IMF sensitivity is the result of the increase of the number of low-mass (low effective temperature) stars relative to high-mass stars.

increasing galaxy velocity dispersion or stellar mass (Cenarro et al. 2003; Conroy & van Dokkum 2012; Ferreras et al. 2013; La Barbera et al. 2013; Spiniello et al. 2014). In addition, radial IMF gradients in local ETGs have been measured (Martín-Navarro et al. 2015; La Barbera et al. 2017; Sarzi et al. 2017; van Dokkum et al. 2017), suggesting that the dwarf-enhanced population is mostly confined to the innermost regions of the galaxy (but see also Alton, Smith & Lucey 2017). It is worth noting that for old systems, such as ETGs, the study of unresolved stellar populations through their integrated light is sensitive only to long-lived stars, i.e. it does not constrain the high-mass-end slope of the IMF (i.e. above $\sim 1\,\mathrm{M}_{\odot}$). Moreover, IMF-sensitive features are mostly sensitive to the dwarf-to-giant ratio in the IMF (La Barbera et al. 2013, hereafter LB13), although the IMF shape might be constrained in detail by combining features at different wavelengths (Conroy & van Dokkum 2012; La Barbera et al. 2016; Lyubenova et al. 2016).

Possible IMF variations as a function of galaxy star formation rate (SFR) activity have been often proposed in the literature. Based on the analysis of optical colours and $H\alpha$ line-strengths for galaxies in the Galaxy And Mass Assembly (GAMA) survey, Gunawardhana et al. (2011) found evidence for a flatter IMF *high-mass* slope in systems with higher SFR. From a theoretical point of view, strongly star-forming regions are expected to have the largest deviations with respect to a universal, MW-like, IMF (see e.g. Klessen et al. 2005). Weidner & Kroupa (2005) proposed a derivation of the integrated galaxy-wide stellar IMF (IGIMF), based on a limited number of physically and observationally motivated axioms. It is possible to reformulate each of these as a function of SFR and thus predict the IMF shape as a function of this key physical property of galaxies. The original IGIMF approach postulates the universality of the IMF inside individual molecular clouds (MCs), with the variability being driven by additional assumptions on the distribution of MCs in the galaxy and by physical considerations on the mass of the most-massive star that can form in a given MC. These assumptions translate into an invariant shape for the low-mass end of the IGIMF, which is at variance with results obtained from the spectra of ETGs (but see Jerabkova et al., in preparation for a recent update of the IGIMF framework). A different approach has been taken by Papadopoulos et al. (2011, P11 hereafter), who consider the role of cosmic rays (CRs), associated with SNe and stellar winds, in regulating star formation in MCs. CRs are assumed to be very effective in altering the thermal and chemical properties of the inner – UV shielded – regions of MCs, eventually changing the relation between gas density and temperature in MC cores. The characteristic Jeans mass of young stars ($M_{\mathrm{J}}^{\star}$) forming in each MC is thus affected. P11 discuss numerical solutions to the thermal and chemical equations describing the evolution of the interstellar medium in this scenario (see also Thi et al. 2009). These numerical solutions provide an estimate for $M_{\mathrm{J}}^{\star}$ as a function of cluster core density ρ_{cl} and CR ionization rate.

Although featuring a different evolution of the IMF shape (in the IGIMF framework, the evolution is mainly tied to the high-mass end, whereas in the CR approach to the knee of the mass function), both models predict similar variations in strongly star-forming objects, i.e. the IMF should become 'top-heavier', at the high-mass end, than in the local neighbourhood at increasing SFR or CR energy density. In previous work, we tested the impact of the IGIMF (Fontanot et al. 2017, F17 hereafter) and CR regulation (Fontanot et al. 2018, F18 hereafter) on the evolution of the physical and chemical properties of galaxies, as predicted by the semi-analytic model GAEA (GAlaxy Evolution and Assembly – Hirschmann, De Lucia & Fontanot 2016). We have shown that in both frameworks we reproduce a mass and mass-to-light ratio excess (Cappellari et al. 2012; Conroy et al. 2013) with respect to a MW-like IMF, which we interpret as driven by the mismatch between intrinsic physical properties and those derived from synthetic photometry under the assumption of a universal IMF. In addition, in both scenarios we are able to reproduce, at the same time, the observed increase for the [α/Fe] ratio as a function of galaxy stellar mass and the mass–metallicity relation of ETGs. Matching both observables represents a known problem for hierarchical models implementing a universal IMF (De Lucia, Fontanot & Hirschmann 2017). In particular, reproducing the [α/Fe]–$M_{\star}$ relation requires a balancing between the relative number of Type-II and Type-Ia SNe, contributing to most of the α-elements and iron, respectively. Assuming a 'top-heavy' IMF at increasing SFR helps matching the observations, as it implies a larger fraction of Type-II SNe in strong starbursts (associated with massive galaxies). However, that is in contrast with the finding of a 'bottom-heavy' IMF in massive galaxies. On the other hand, a 'bottom-heavy' IMF with a slope steeper than Salpeter over the entire stellar mass range implies a low fraction of Type-II SNe and this is in contrast with the observed metallicity and abundance ratios of massive galaxies. These considerations are even more puzzling in light of recent studies finding IMF radial trends in ETGs, with a steepening of the IMF low-mass-end slope in the innermost, more metal-rich, galaxy core regions. In order to reconcile these apparently contradicting results, Weidner et al. (2013) and Ferreras et al. (2015, see also Vazdekis et al. 1996) have proposed a time-varying scenario, where the low- and high-mass ends of the IMF vary independently over different time scales, with the top-heavy regime dominating the first (bursty) phase of star formation, followed by a bottom-heavy regime. The implications of such a variable IMF for ETG chemical evolution have been explored, e.g. in De Masi et al. (2018). However, a physical explanation for this time-varying scenario, possibly related to the complex physics of gas fragmentation in the dense core regions of massive galaxies at high redshift, is still lacking.

In this work, we combine the IGIMF and P11 approaches to derive a new formulation for the IGIMF that takes into account explicitly the effect of CR heating on the IMF of individual MCs. We present this new combined derivation, which we dubbed CR-IGIMF, in Section 2, we show its basic properties in Section 3, and we then discuss our results and their implications in Section 4.

2 COSMIC-RAYS-REGULATED IGIMF

In this paper, we present a derivation of the IGIMF (φ_{IGIMF}) based on an approach similar to Weidner & Kroupa (2005, see also Kroupa et al. 2013 for a review). We integrate the IMF associated with individual clouds ($\varphi_{\star}(m)$), weighted by the mass function of individual MCs ($\varphi_{\mathrm{CL}}(M_{\mathrm{cl}})$):

$$\varphi_{\mathrm{IGIMF}}(m) = \int_{M_{\mathrm{cl}}^{\mathrm{min}}}^{M_{\mathrm{cl}}^{\mathrm{max}}} \varphi_{\star}(m \leq m_{\star}^{\mathrm{max}}(M_{\mathrm{cl}}))\varphi_{\mathrm{CL}}(M_{\mathrm{cl}})\,\mathrm{d}M_{\mathrm{cl}}. \quad (1)$$

The key quantities involved in the integration are the maximum value of the mass of a star cluster ($M_{\mathrm{cl}}^{\mathrm{max}}$) and the largest stellar mass (m_{max}) forming in a given cluster. We set the mass of the smallest star cluster to $M_{\mathrm{cl}}^{\mathrm{min}} = 5\,\mathrm{M}_{\odot}$ following pieces of evidence from the Taurus–Auriga complex (Kroupa & Bouvier 2003). As in F17, $M_{\mathrm{cl}}^{\mathrm{max}}$ and m_{max} can be defined as a function of the instantaneous SFR using the following axioms:

$$\log M_{\mathrm{cl}}^{\mathrm{max}} = 0.746 \log \mathrm{SFR} + 4.93; \quad (2)$$

$$\log m_{\star}^{\rm max} = 2.56\,\log M_{\rm cl}[\,3.82^{9.17} + (\log M_{\rm cl})^{9.17}\,]^{1/9.17} - 0.38; \quad (3)$$

$$\varphi_{\rm CL}(M_{\rm cl}) \propto M_{\rm cl}^{-\beta}; \quad (4)$$

$$\beta = \begin{cases} 2 & {\rm SFR} < 1\,{\rm M}_{\odot}\,{\rm yr}^{-1} \\ -1.06\log {\rm SFR} + 2 & {\rm SFR} \geq 1\,{\rm M}_{\odot}\,{\rm yr}^{-1} \end{cases}; \quad (5)$$

$$\alpha_3 = \begin{cases} 2.35 & \rho_{\rm cl} < 9.5\times10^4\,{\rm M}_{\odot}\,{\rm pc}^{-3} \\ 1.86 - 0.43\log(\frac{\rho_{\rm cl}}{10^4}) & \rho_{\rm cl} \geq 9.5\times10^4\,{\rm M}_{\odot}\,{\rm pc}^{-3} \end{cases}; \quad (6)$$

$$\log \rho_{\rm cl} = 0.61\log M_{\rm cl} + 2.85. \quad (7)$$

Using stellar cluster data, Weidner, Kroupa & Larsen (2004) derived equation (2) to describe the dependence of $M_{\rm cl}^{\rm max}$ on the instantaneous SFR (see also Kroupa et al. 2013 for an analytic derivation). As in F17, we impose[2] $M_{\rm cl}^{\rm max} \leq 2\times10^7\,{\rm M}_{\odot}$. Equation (3) represents a fit to the numerical solution to the problem of finding the maximum stellar mass forming in a cluster of mass $M_{\rm cl}$ (Pflamm-Altenburg, Weidner & Kroupa 2007), under the hypothesis that it contains exactly one $m_{\rm max}$ star and using the canonical IMF. Equation (4) describes the assumed functional shape for the star cluster mass function. Allowed values for β (equation 5) are chosen on the basis of local observations that suggest $\beta = 2$ (Lada & Lada 2003) and on $z \lesssim 0.35$ data from the GAMA survey (Gunawardhana et al. 2011) that require a flattening of β at high SFRs. Equation (6) takes into account possible variations of the high-mass-end slope α_3 from the reference choice $\alpha_3 = 2.35$ (see Kroupa et al. 2013 for a review). As in F17, in this work, we assume that α_3 depends on $\rho_{\rm cl}$, as proposed by Marks et al. (2012). This relation has the advantage of being independent of other parameters (such as metallicity) that have been shown to also correlate with α_3 (see e.g. Martín-Navarro et al. 2015). Finally, equation (7) describes the relation between $\rho_{\rm cl}$ and $M_{\rm cl}$, as derived by Marks & Kroupa (2012).

Using the above-mentioned equations, and assuming a given $\varphi_{\star}(m)$ for individual MCs, it is then possible to construct the IGIMF corresponding to an individual star formation (SF) event. In the original Weidner & Kroupa (2005) framework, the IMF associated with individual MCs has a canonical broken power-law shape with three slopes (as in Kroupa 2001; see equation 1 in F17). In this paper, we use a slightly different approach by considering a variable inner break at $m_{\rm br}$:

$$\varphi_{\star}(m) = \begin{cases} (\frac{m}{m_{\rm low}})^{-\alpha_1} & m_{\rm low} \leq m < m_{\rm br} \\ (\frac{m_{\rm br}}{m_{\rm low}})^{-\alpha_1}(\frac{m}{m_{\rm br}})^{-\alpha_2} & m_{\rm br} \leq m < m_1 \\ (\frac{m_{\rm br}}{m_{\rm low}})^{-\alpha_1}(\frac{m_1}{m_{\rm br}})^{-\alpha_2}(\frac{m}{m_1})^{-\alpha_3} & m_1 \leq m \leq m_{\rm max} \end{cases}, \quad (8)$$

where the parameters $m_{\rm low} = 0.1$, $m_1 = 1.0$, $\alpha_1 = 1.3$, and $\alpha_2 = 2.35$ are fixed. The position of the break at $m_{\rm br}$ is derived using the approach of P11, assuming that it corresponds to the characteristic Jeans mass ($M_{\rm J}^{\star}$) of young stars in an MC with core density given by equation (7), and affected by the CR energy density $U_{\rm CR}$. Whereas in F18 we fixed the knee to the value of $M_{\rm J}^{\star}$ for a typical density $\rho_{\rm cl} = 10^5\,{\rm cm}^{-3}$, in this paper we use a different approach, considering a grid of values

$$m_{\rm br} = M_{\rm J}^{\star}(\rho_{\rm cl}, U_{\rm CR}). \quad (9)$$

For practical reasons, we use the numerical solutions to the chemical and thermal equations for the CR-regulated ISM presented in fig. 4 of P11. These numerical experiments provide indeed interesting insights on the key physical dependences. In particular, $m_{\rm br}$ increases with $U_{\rm CR}$: This is mainly due to the higher CR heating associated with the increased energy density. At fixed $U_{\rm CR}$, $m_{\rm br}$ is predicted to decrease with $\rho_{\rm cl}$. This behaviour is not trivial, as high-density regions are expected to be generally hotter, and the Jeans mass increases with temperature and decreases with density. Hence, in the numerical treatment of P11, the dependence on temperature appears subdominant with respect to that on density. The effect is important in our analysis, as it allows changes in the low-mass-end slope of the IGIMF (as discussed below). In the following section, we use the same notation as in P11, and consider $U_{\rm CR}$ values relative to the corresponding MW one ($U_{\rm MW}$).

3 PROPERTIES OF THE CR-IGIMF

We can now compute the IGIMF shape as a function of both SFR and $U_{\rm CR}/U_{\rm MW}$. It is important to keep in mind that the original P11 approach focuses on individual MCs and SFR and $U_{\rm CR}/U_{\rm MW}$ are treated as independent variables ($U_{\rm CR}$ represents an external field). Our combined approach, instead, considers both SFR and $U_{\rm CR}$ as 'global' variables, given by an average over SF regions. Therefore, in our implementation, SFR and $U_{\rm CR}/U_{\rm MW}$ are not completely independent variables.[3] In Fig. 1, we show some representative IMF shapes. Each panel refers to a different value of $U_{\rm CR}/U_{\rm MW}$, and three different SFR values (100, 1, and 0.01 ${\rm M}_{\odot}\,{\rm yr}^{-1}$), each normalized to $1\,{\rm M}_{\odot}$. Fig. 1 shows that the CR-IGIMF framework features a variety of IMF shapes, while for an SF galaxy with MW-like energy density field it predicts an IMF shape that is in good agreement with a Kroupa-like IMF (green solid line in the middle-upper panel). At fixed $U_{\rm CR}/U_{\rm MW}$, the high-mass end becomes shallower at increasing SFR, as in the original IGIMF approach. We thus expect that a model implementing the CR-IGIMF should be able to reproduce the observed trend in the [α/Fe]–stellar mass relation of ETGs (see e.g. Thomas et al. 2010). At the low-mass end, the situation is more complex and depends on $U_{\rm CR}$. For CR densities much higher than in the MW, the low-mass-end slope is constant, whereas for $U_{\rm CR}/U_{\rm MW} \lesssim 10$ there is a clear trend for a steepening of the IMF at increasing SFR. By construction (see above), the minimum and maximum slopes for the low-mass end of the CR-IGIMF are α_1 and α_2. In our approach, α_1 and α_2 assume a fixed value (1.3 and a Salpeter-like slope of 2.35). This is a conservative choice, which complies with both local observations of individual clouds and with theoretical calculations of the fragmentation of giant MCs (Hennebelle & Chabrier 2008). However, we note that there is no physical reason for these slopes to be the same for MCs evolving in physical conditions very different from those in the MW. Indeed, variations in the IMF shape of individual MCs have been considered in the original IGIMF framework (see e.g. Yan, Jerabkova & Kroupa 2017). In particular, equation (6) follows an empirical calibration connecting

[2] This value is consistent with the idea that present Globular Clusters might have had up to a factor 100 higher mass at birth (Weidner et al. 2004). Whereas the exact value clearly depends on the IGIMF, we choose a rather conservative value. It is worth stressing that equation (2) predicts values larger than $M_{\rm cl}^{\rm max}$ only for SFR $\geq 10^{3.5}\,{\rm M}_{\odot}\,{\rm yr}^{-1}$. In F17 and F18, we show that such strong SF events are not typical in theoretical models implementing a variable IMF.

[3] F18 assumed that $U_{\rm CR}$ is homogeneous within model galaxies and proportional to the total disc SFR surface density ($\Sigma_{\rm SFR}$). As shown in fig. 3 of F18, galaxies populate well-defined regions in the SFR–$\Sigma_{\rm SFR}$ space.

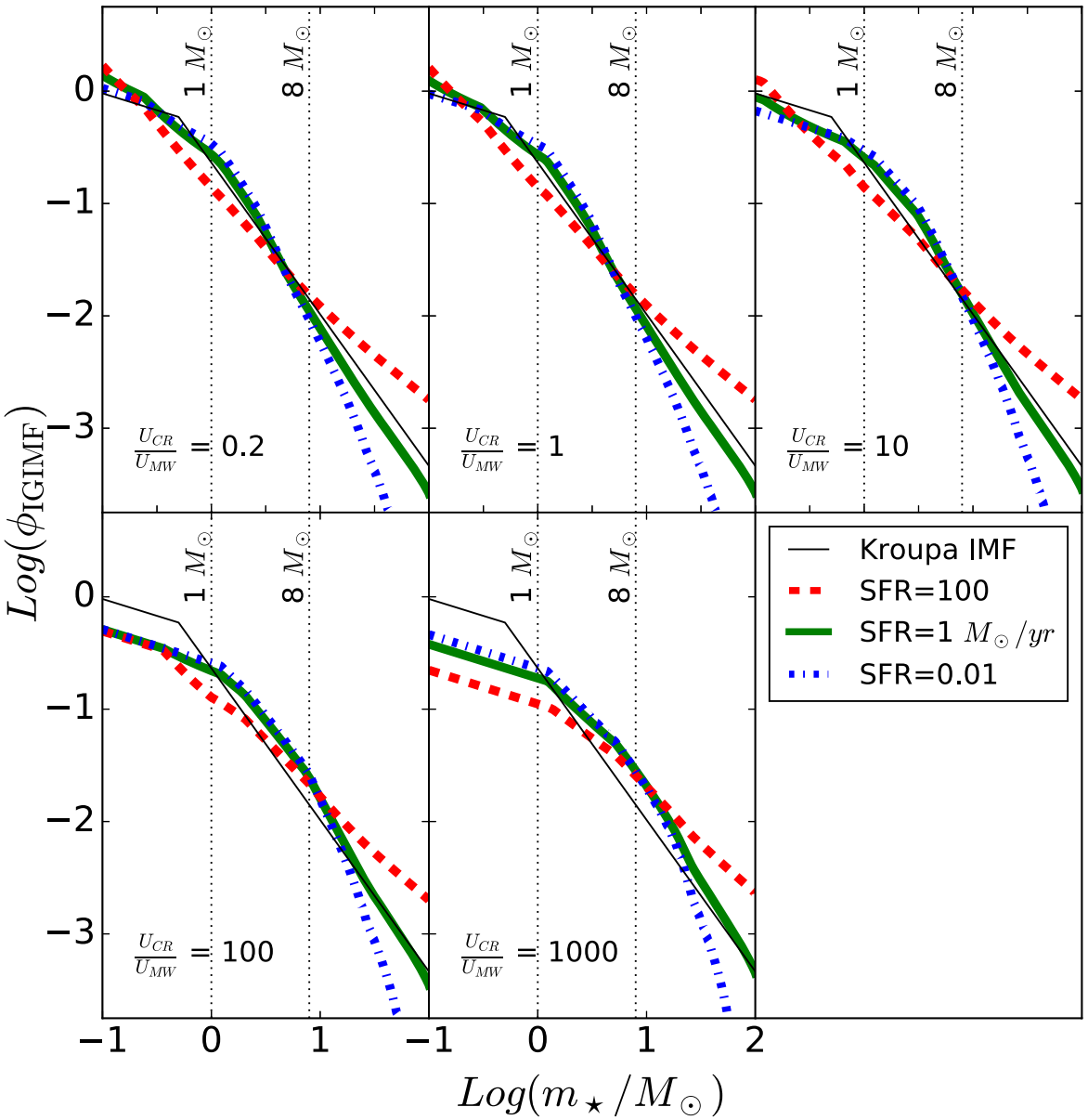

Figure 1. Composite shapes for the CR-regulated IGIMF. Different panels refer to different CR energy densities, as labelled in the lower-left corner of each panel. Red-dashed, green solid and blue-dotted lines correspond to SFR = 100, 1, and 0.01 $M_\odot$ yr^{-1}, respectively. In all panels, the thin solid line shows the canonical Kroupa (2001) IMF.

the IMF high-mass-end slope and the observed properties of local MCs (Marks et al. 2012). None the less, as shown explicitly in P11, the impact of $U_{\rm CR}$ on $M_{\rm J}^\star$ is such that it can also affect the IMF shape of individual clouds for $m_\star \lesssim 1\,{\rm M}_\odot$. Our approach accounts for this effect, thus assuming that CRs can affect the IMF shape on a wider stellar mass range than in the original IGIMF formulation.

For a MW-like $U_{\rm CR}$ environment, high-SFR events correspond to a steeper low-mass-end slope and to a shallower high-mass-end slope with respect to a Kroupa IMF, *at the same time*. Therefore, our implementation of the CR-IGIMF should explain the enhanced fraction of low-mass-to-giant stars inferred from IMF-sensitive features in the spectra of ETGs (Conroy & van Dokkum 2012; La Barbera et al. 2017; Sarzi et al. 2017), while qualitatively preserving most of the results discussed in F17 and F18. Analysing these aspects in detail requires a self-consistent theoretical model including explicitly the effects of the CR-IGIMF. In this work, we present a preliminary analysis focusing on the mass fraction of low-mass stars ($f_{\rm dg}$), defined as the fraction of mass in stars with $m_\star < 0.6\,{\rm M}_\odot$, with respect to the total mass in stars $m_\star < 1.0\,{\rm M}_\odot$.

The value $f_{\rm dg}$ represents the dwarf-to-giant ratio, which is the main quantity constrained by IMF-sensitive spectral features in the spectra of $z \sim 0$ ETGs. Using a large Sloan Digital Sky Survey (SDSS) sample of ETGs, Ferreras et al. (2013) and LB13 constructed 18 stacked galaxy spectra, covering a velocity dispersion range from ∼100 to ∼300 km s^{-1}. The authors found a systematic steepening of the low-mass end as a function of galaxy velocity dispersion and parameterized the IMF by either a single power-law (unimodal) or a low-mass-tapered (bimodal) distribution. We consider here results of the '2SSP+XFe' fitting method of LB13, in which spectral indices are fitted with stel-

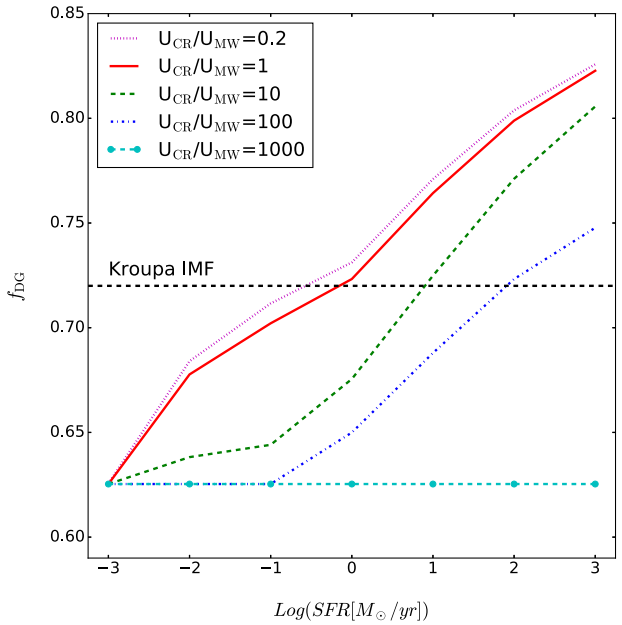

Figure 2. Fraction of dwarf-to-giant stars, $f_{\rm dg}$, for individual CR-regulated IGIMFs (see the text for details). Different lines correspond to different CR densities, as labelled in the upper-left corner of the figure. The horizontal black -dashed line shows the $f_{\rm dg}$ value for a MW-like Kroupa IMF.

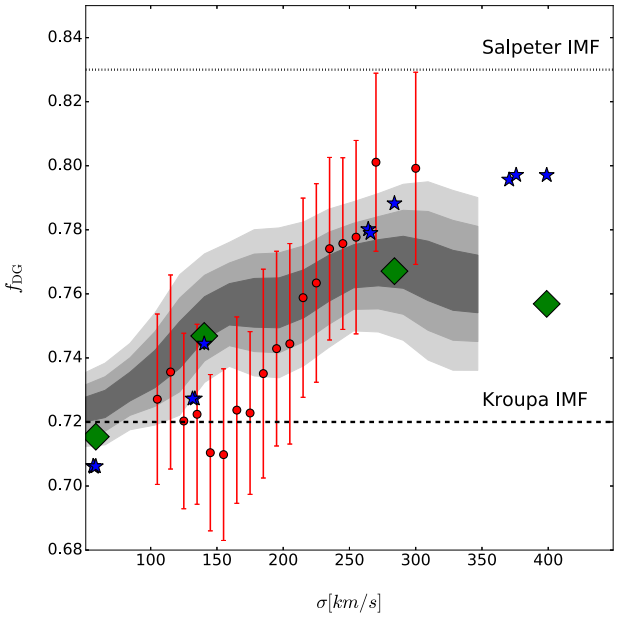

Figure 3. The expected fraction of dwarf-to-giant stars, $f_{\rm dg}$, is plotted against galaxy velocity dispersion for mock SFHs extracted from semi-analytic models. Red bullets with error bars show the observational constraints from LB13, after correcting $f_{\rm dg}$ to an aperture of 1 effective radius by assuming IMF radial gradients as in La Barbera et al. (2017). Blue stars are predicted values of $f_{\rm dg}$ for mean SFHs extracted from GAEA, in reference stellar mass bins (i.e. $M_\star \sim 10^{12}$, $10^{11.5}$, $10^{10.5}$, and $10^{9.25}$ $M_\odot$, respectively), and assuming a fixed $U_{\rm CR}/U_{\rm MW} = 1$. Grey-shaded areas correspond to 1σ, 2σ, and 3σ levels around the mean $f_{\rm dg}$ versus σ relation for the mocks galaxy sample extracted from the P11 run, while green diamonds correspond to the predictions for mean SFHs in our reference mass bins (see the text for details).

lar population models including two single stellar populations (SSPs) and accounting for the effect of non-solar abundance ratios. As shown in LB13, both unimodal and bimodal models fit equally well the data but provide very different mass-to-light ratio estimates. The two IMF parameterizations provide, however, very similar dwarf-to-giant fractions. Computing $f_{\rm dg}$ from the LB13 '2SSP+XFe' results, we find values ranging between 0.6 and 0.95. These values refer to the inner core regions of ETGs, as observed by the SDSS fibre aperture spectra. For galaxies in the highest mass bin considered in LB13, this aperture corresponds to about 1/4 of a galaxy effective radius. We compute $f_{\rm dg}$ for individual CR-IGIMFs, using a grid of 42 independent realizations, with seven SFR levels (with $\log({\rm SFR}/\,{\rm M}_\odot\ {\rm yr}^{-1}) =$, -3, -2, -1, 0, 1, 2, and 3) and six $U_{\rm CR}/U_{\rm MW}$ values (0.2, 1, 10, 100, 1000, and 10000, as in P11). On this CR-IGIMF grid, $f_{\rm dg}$ ranges between 0.6 and 0.8, as shown in Fig. 2. The reason for this range of values is that, by construction (see equation 8), no CR-IGIMF in our approach can have a slope steeper than $\alpha_2 = 2.35$ (i.e. a Salpeter IMF) or shallower than $\alpha_1 = 1.3$. For single power-law IMFs, these slopes correspond to $f_{\rm dg} = 0.84$ (α_2) and 0.6 (α_1), respectively. The figure shows a clear trend for an increase of $f_{\rm dg}$ with SFR at fixed $U_{\rm CR} < 100$. Vice versa, $f_{\rm dg}$ decreases with increasing U, at fixed SFR. In particular, for CR density values larger than 100 times that of the MW, the low-mass-end slope of the IMF is constant, with ratios below the expectation for a Kroupa IMF. In order to get $f_{\rm dg}$ values as high as 0.95 (found for the core regions of the most-massive ETGs in the LB13 sample), one should postulate that also the intrinsic IMF for individual MCs should assume 'super'-Salpeter slopes under specific physical conditions (e.g. for high-metallicity/density environments; see Martín-Navarro et al. 2015).

4 RESULTS AND DISCUSSION

The crucial aspect we want to test in this work is whether the CR-IGIMF scenario, once embedded in a realistic galaxy formation context, can match the observed trends. To this purpose, we use mean star formation histories (SFHs) predicted by the GAEA semi-analytic model (Hirschmann et al. 2016) for $z = 0$ galaxies in four different stellar mass bins, namely $M_\star \sim 10^{12}$, $10^{11.5}$, $10^{10.5}$, and $10^{9.25}$ $M_\odot$. These SFHs have been extracted from the reference GAEA realization and from runs implementing variable IMF approaches (F17 and F18). Galaxies more massive than $\sim 10^{10.5}$ are typically characterized by an early peak of SFR, followed by a smooth decay. The epoch, height, and width of the peak depend on the final galaxy stellar mass, with more massive galaxies having an earlier, narrower, and higher peak (see also De Lucia et al. 2006). Lower mass galaxies have almost constant SFHs. For the mean SFH in each mass bin, we compute the mass-weighted global IMF using our CR-IGIMF grid and then the corresponding value of $f_{\rm dg}$. It is worth noting that in our estimate for $f_{\rm dg}$ we only consider the $< 1\,{\rm M}_\odot$ mass range, where the mass-weighted IMF coincides with the present-day mass function. Moreover, observational constraints are closer to luminosity-weighted IMFs. However, for very old stellar populations (i.e. massive ETGs), we do not expect this difference to change our conclusions significantly. In Fig. 3, we compare these $f_{\rm dg}$ for $U_{\rm CR}/U_{\rm MW} = 1$ (blue stars – for each mass bin, we plot separately the values corresponding to the mean SFHs extracted from the three GAEA realizations considered), with the observed values. We correct the observed values of $f_{\rm dg}$ from LB13 to an aperture of 1 effective radius, whose properties we consider to be comparable to SAM predictions. To this aim, we assume an IMF radial profile with the same shape as that recently derived for one massive ETG by La Barbera et al. (2017). For each mass bin,

the profile is rescaled, in the central region, in order to match the f_{dg} value within the SDSS fibre aperture, as detailed in LB13. The correction, which is larger at the highest mass and negligible at the lowest mass,[4] brings all f_{dg} values from LB13 in the range from ∼0.72 to ∼0.8, as illustrated in Fig. 3 (see red dots with error bars, corresponding to the 18 stacked spectra of LB13). Remarkably, the aperture correction brings the observed f_{dg} values within the range predicted by the CR-IGIMF.

For model galaxies, we estimate σ using the stellar mass–σ relation derived by Zahid et al. (2016), and compute stellar masses from the SFHs under the hypothesis of a Kroupa IMF, consistently with the adopted mass–σ relation. We checked that our conclusions hold if we estimate the actual stellar mass associated with the adopted SFHs, i.e. using the actual IMF shape and appropriate mass fraction locked into stellar remnants for each varying IMF. Model predictions with $U_{CR}/U_{MW} = 1$ reproduce well the trend of increasing f_{dg} with σ. We verified that this applies also to models with fixed $U_{CR}/U_{MW} \lesssim 10$. We finally relax the hypothesis of a uniform U_{CR}/U_{MW} for our toy SFHs, and we consider predictions from the GAEA run implementing the P11 approach (as defined in F18). In this run, we are able to track at the same time the evolution of SFR and Σ_{SFR} for each model galaxy. As in F18, we assume $U_{CR}/U_{MW} = \Sigma_{SFR}/\Sigma_{MW}$, i.e. that the SFR density is a good proxy for U_{CR} over the star-forming disc. We then compute the mean SFRs and SFR densities as a function of cosmic time in our reference mass bins. We also extract individual SFHs and SFR density histories for ∼380 000 individual $z = 0$ model galaxies from the same realization. This information allows us to follow the time evolution of our model galaxies in the CR-IGIMF library. Fig. 3 shows the resulting f_{dg} as a function of σ. Green diamonds mark average values corresponding to the four reference mass bins. The grey areas correspond to the 1σ, 2σ, and 3σ levels around the mean relation for the mock galaxies sample extracted from the P11 run, which nicely match the (aperture-corrected) trend of increasing f_{dg} with σ obtained by LB13. Interestingly, the trend is predicted to flatten at the highest stellar mass bin probed by the F18 models, although the number of mock galaxies in this range is small. This is mainly due to the fact that more-massive galaxies in F18 form preferentially in strong compact starburst, with high SFR and Σ_{SFR}, that correspond to lower f_{dg}. To better highlight this effect, we show in Fig. 4 the different CR-IGIMF shapes at fixed SFR, as a function of U_{CR}/U_{MW}. In our toy SFHs, a massive galaxy is characterized by an early large peak of SF: In these conditions (upper panels in Fig. 4), our CR-IGIMF scenario consistently predicts a shallower high-mass-end slope. The low-mass-end slope, which is mainly responsible for setting f_{dg}, strongly depends on the SFR density (that we use as a proxy for U_{CR}). Therefore, an accurate estimate for the CR energy density is a crucial element to correctly predict the shape of the CR-IGIMF. The late-time evolution of a massive galaxy is associated with low-SFR and low-SFR density, which correspond to shallower low-mass-end slopes (bottom panel of Fig. 4).

In order to further compare predictions from our CR-IGIMF model to observations, we compute synthetic model spectra corresponding to the F18 mean SFHs in the reference mass bins of $M_\star = 10^{9.25}$ and $10^{11.5}$ ($\sigma \sim 60$ and ∼280 km s^{-1}). We consider the MILES[5] stellar library and the Padova 2000 isochrones (Girardi et al. 2000), and we build up the spectral energy distributions (SEDs) by summing up the SSPs corresponding to the mean (mass-weighted) IMF in the CR-IGIMF framework.[6] Since we want to highlight the effect of a varying IMF, rather than other stellar population properties, for both mass bins, we consider the same (old) age of ∼10 Gyr and solar metallicity. Fig. 5 shows, as a thick red curve, the ratio between these toy model spectra for the highest relative to lowest mass bin. This ratio represents the IMF signal corresponding to the CR-IGIMF implementation applied to F18 mean SFHs. The figure plots the wavelength range from 5800 to ∼6700 Å, where several IMF-sensitive features (like TiO1 and TiO2) are located (as marked in the plot). The thin black line in Fig. 5 represents the 'observed' IMF signal, obtained by dividing a bimodal SSP MILES model (Vazdekis et al. 2010) with slope $\Gamma_b = 1.8$ (that should well describe massive galaxies), to that for a Kroupa IMF (that well describes the lowest mass stacks of LB13). In deriving the thin black line, we account for aperture correction in real data and we consider SSPs with the same age and metallicity as those used for the mean F18 SFHs. Fig. 5 shows that the CR-IGIMF and 'observed' IMF variations from low- to high-mass galaxies agree reasonably well, consistent with what is seen in Fig. 3, for the dwarf-to-giant ratio, f_{dg}.

The results shown in Figs. 3 and 5 are based on SFHs extracted from GAEA runs, hence implementing a different varying-IMF approach than the CR-IGIMF framework described here. In F18, we have shown that a varying-IMF scenario can significantly affect

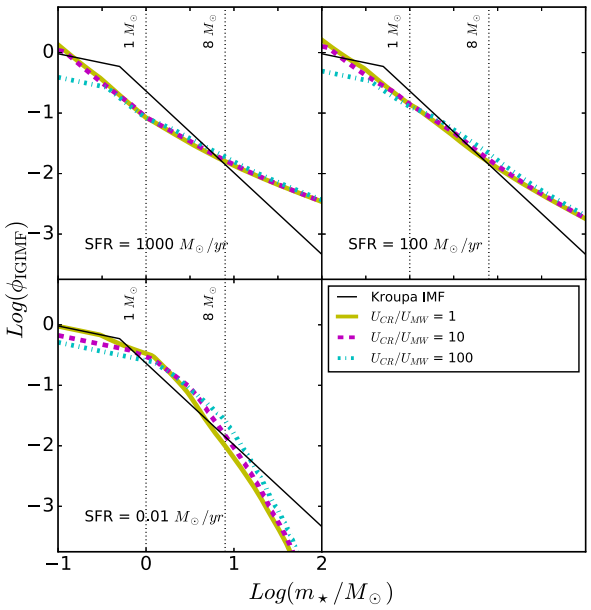

Figure 4. Same as in Fig. 1, but different panels refer to different SFR levels, as labelled in the lower-left corner of each panel. Yellow solid, magenta-dashed and cyan-dotted lines correspond to U_{CR}/U_{MW} =1, 10, and 100, respectively. In all panels, the thin solid line shows the canonical Kroupa (2001) IMF.

[4]It is worth noting that this approach is consistent with recent findings that lowest mass galaxies have shallower gradients compared to the most-massive ones (Martín-Navarro et al. 2015; Parikh et al. 2018).

[5]miles.iac.es

[6]In order to obtain the desired values of metallicity, gravity, and effective temperature, we interpolate MILES spectra using the same algorithm as in Vazdekis et al. (2010). We then weight the interpolated spectra using the mass–(*V*-band)luminosity relation, rather than using empirical relations (as in Vazdekis et al. 2010). Therefore, the resulting SSPs should be regarded as simple toy models and not full MILES SSP SEDs.

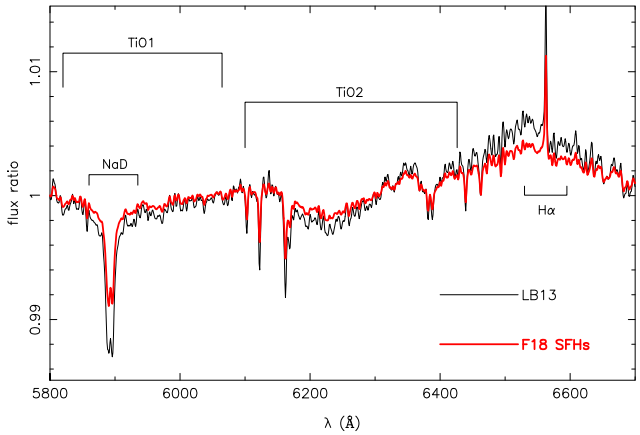

Figure 5. The thick red line shows the ratio between toy model spectra corresponding to the $M_\star = 10^{9.25}$ and $10^{11.5}\,M_\odot$ F18 galaxies in the CR-IGIMF scenario. This is compared to the observed IMF variation signal in similar mass bins, i.e. the ratio of MILES SSP models that better describes observations from LB13, after applying an aperture correction, as detailed in the text. Horizontal brackets, with labels, mark several IMF-sensitive features in the plotted spectral range.

galaxy evolution, as predicted by GAEA, since it changes the IMF that we associate with each individual SF event predicted by the model. A model implementing a variable IMF such as the CR-IGIMF thus implies a time variation of the IMF: This effect has deep implications for the predicted SFHs of the different galaxy populations (see e.g. Ferré-Mateu, Vazdekis & de la Rosa 2013). Therefore, the development of a self-consistent version of GAEA, implementing the CR-IGIMF, is desirable and will be presented in a future work. Such a model would allow us to carry out a more detailed comparison with observational data, including a direct comparison of synthetic spectra for our mock galaxies with observed ones. Another aspect that deserves further investigation is that of IMF radial gradients in ETGs. We expect the central regions (i.e. those showing a stronger signal for a 'bottom-heavy' IMF) to have larger SFRs and SFR densities, with respect to the galaxy outskirts. Naively, in the current CR-IGIMF implementation, we would tend to associate a lower $f_{\rm dg}$ to these regions, in contrast to some recent observational results (Martín-Navarro et al. 2015; La Barbera et al. 2016; Sarzi et al. 2017; van Dokkum et al. 2017). Again, a self-consistent version of GAEA implementing the CR-IGIMF is clearly needed to study this aspect, taking into account the different star-forming regions associated with the hierarchical assembly of massive ETGs and their individual IMFs. Moreover, as mentioned above, one should consider that specific physical properties (e.g. metallicity – see Martín-Navarro et al. 2015) may affect the IMF of individual MCs in the core regions of massive ETGs, hence requiring further modifications to the CR-IGIMF framework.

The results presented in this work are meant to show the capabilities of the CR-IGIMF approach in a galaxy evolution framework. Our models predict $f_{\rm dg}$ values, over a spatial scale comparable to that of galaxy sizes, that are consistent with the observed ones. This demonstrates that the CR-IGIMF scenario is able to capture key features of the IMF low- and high-mass end that have been elusive so far. Forthcoming work will focus on the development of theoretical models self-consistently including both the effect of CR-IGIMF on model galaxy evolution and the synthesis of realistic mock spectra. This work shows that these tools are of fundamental importance for interpreting the wealth of observational data in favour of a variable IMF.

ACKNOWLEDGEMENTS

FF thanks P. Kroupa for stimulating discussions on the definition of the IGIMF framework. GDL thanks the Alexander von Humboldt Foundation and the Astronomisches Rechen-Institut of Heidelberg for the pleasant and productive stay during which part of this work was carried out. FLB and AV acknowledge support from grant AYA2016-77237-C3-1-P from the Spanish Ministry of Economy and Competitiveness (MINECO).

REFERENCES

Alton P. D., Smith R. J., Lucey J. R., 2017, MNRAS, 468, 1594
Cappellari M. et al., 2012, Nature, 484, 485
Cenarro A. J., Gorgas J., Vazdekis A., Cardiel N., Peletier R. F., 2003, MNRAS, 339, L12
Conroy C., van Dokkum P. G., 2012, ApJ, 760, 71
Conroy C., Dutton A. A., Graves G. J., Mendel J. T., van Dokkum P. G., 2013, ApJ, 776, L26
De Lucia G., Springel V., White S. D. M., Croton D., Kauffmann G., 2006, MNRAS, 366, 499
De Lucia G., Fontanot F., Hirschmann M., 2017, MNRAS, 466, L88
De Masi C., , Vincenzo F., Matteucci F., Rosani G., Barbera L., Pasquali A., Spitoni E., 2018, preprint (arXiv:1805.06841)
Dutton A. A., Macciò A. V., Mendel J. T., Simard L., 2013, MNRAS, 432, 2496
Faber S. M., French H. B., 1980, ApJ, 235, 405
Ferré-Mateu A., Vazdekis A., de la Rosa I. G., 2013, MNRAS, 431, 440
Ferreras I., La Barbera F., de la Rosa I. G., Vazdekis A., de Carvalho R. R., Falcón-Barroso J., Ricciardelli E., 2013, MNRAS, 429, L15
Ferreras I., Weidner C., Vazdekis A., La Barbera F., 2015, MNRAS, 448, L82
Fontanot F., De Lucia G., Hirschmann M., Bruzual G., Charlot S., Zibetti S., 2017, MNRAS, 464, 3812 (F17)
Fontanot F., De Lucia G., Xie L., Hirschmann M., Bruzual G., Charlot S., 2018, MNRAS, 475, 2467 (F18)
Girardi L., Bressan A., Bertelli G., Chiosi C., 2000, A&AS, 141, 371
Gunawardhana M. L. P. et al., 2011, MNRAS, 415, 1647
Hennebelle P., Chabrier G., 2008, ApJ, 684, 395
Hirschmann M., De Lucia G., Fontanot F., 2016, MNRAS, 461, 1760
Klessen R. S., Ballesteros-Paredes J., Vázquez-Semadeni E., Durán-Rojas C., 2005, ApJ, 620, 786
Kroupa P., 2001, MNRAS, 322, 231
Kroupa P., Bouvier J., 2003, MNRAS, 346, 369
Kroupa P., Weidner C., Pflamm-Altenburg J., Thies I., Dabringhausen J., Marks M., Maschberger T., 2013, Planets, Stars and Stellar Systems. Volume 5: Galactic Structure and Stellar Populations. Springer, Dordrecht
La Barbera F., Ferreras I., Vazdekis A., de la Rosa I. G., de Carvalho R. R., Trevisan M., Falcón-Barroso J., Ricciardelli E., 2013, MNRAS, 433, 3017 (LB13)
La Barbera F., Vazdekis A., Ferreras I., Pasquali A., Cappellari M., Martín-Navarro I., Schönebeck F., Falcón-Barroso J., 2016, MNRAS, 457, 1468
La Barbera F., Vazdekis A., Ferreras I., Pasquali A., Allende Prieto C., Röck B., Aguado D. S., Peletier R. F., 2017, MNRAS, 464, 3597
Lada C. J., Lada E. A., 2003, ARA&A, 41, 57
Lyubenova M. et al., 2016, MNRAS, 463, 3220
Marks M., Kroupa P., 2012, A&A, 543, A8
Marks M., Kroupa P., Dabringhausen J., Pawlowski M. S., 2012, MNRAS, 422, 2246
Martín-Navarro I., La Barbera F., Vazdekis A., Falcón-Barroso J., Ferreras I., 2015, MNRAS, 447, 1033

Papadopoulos P. P., Thi W.-F., Miniati F., Viti S., 2011, MNRAS, 414, 1705 (P11)
Parikh T. et al., 2018, MNRAS, 477, 3954
Pflamm-Altenburg J., Weidner C., Kroupa P., 2007, ApJ, 671, 1550
Sarzi M., , Spiniello C., La Barbera F., Krajnović D., van den Bosch R., 2018, MNRAS, 478, 4084
Schiavon R. P., Barbuy B., Rossi S. C. F., Milone A., 1997, ApJ, 479, 902
Schiavon R. P., Barbuy B., Singh P. D., 1997, ApJ, 484, 499
Spiniello C., Trager S., Koopmans L. V. E., Conroy C., 2014, MNRAS, 438, 1483
Thi W.-F., van Dishoeck E. F., Bell T., Viti S., Black J., 2009, MNRAS, 400, 622
Thomas D., Maraston C., Schawinski K., Sarzi M., Silk J., 2010, MNRAS, 404, 1775
Tortora C., La Barbera F., Napolitano N. R., 2016, MNRAS, 455, 308
Trager S. C., Worthey G., Faber S. M., Burstein D., González J. J., 1998, ApJS, 116, 1
Treu T., Auger M. W., Koopmans L. V. E., Gavazzi R., Marshall P. J., Bolton A. S., 2010, ApJ, 709, 1195
van Dokkum P., Conroy C., Villaume A., Brodie J., Romanowsky A. J., 2017, ApJ, 841, 68
Vazdekis A., Casuso E., Peletier R. F., Beckman J. E., 1996, ApJS, 106, 307
Vazdekis A., Sánchez-Blázquez P., Falcón-Barroso J., Cenarro A. J., Beasley M. A., Cardiel N., Gorgas J., Peletier R. F., 2010, MNRAS, 404, 1639
Weidner C., Kroupa P., 2005, ApJ, 625, 754
Weidner C., Kroupa P., Larsen S. S., 2004, MNRAS, 350, 1503
Weidner C., Ferreras I., Vazdekis A., La Barbera F., 2013, MNRAS, 435, 2274
Wing R. F., Ford W. K., Jr, 1969, PASP, 81, 527
Yan Z., Jerabkova T., Kroupa P., 2017, A&A, 607, A126
Zahid H. J., Geller M. J., Fabricant D. G., Hwang H. S., 2016, ApJ, 832, 203

This paper has been typeset from a TEX/LATEX file prepared by the author.